

NACA RM L53I22c

Unclassified

NACA

RESEARCH MEMORANDUM

CLASSIFICATION CANCELLED
Unclassified

Authority *Exec. Res. 12800* Date *9-24-56*
By *J. H. 10-9-56* See *R. N. - 127*

PRESSURE DRAG OF BODIES AT MACH NUMBERS UP TO 2.0

By Robert L. Nelson and William E. Stoney, Jr.

Langley Aeronautical Laboratory
Langley Field, Va.

LANGLEY FIELD, VIRGINIA

CLASSIFIED DOCUMENT

This material contains information affecting the National Defense of the United States within the meaning of the espionage laws, Title 18, U.S.C., Secs. 793 and 794, the transmission or revelation of which in any manner to an unauthorized person is prohibited by law.

NATIONAL ADVISORY COMMITTEE FOR AERONAUTICS

WASHINGTON
November 18, 1953

Unclassified

NATIONAL ADVISORY COMMITTEE FOR AERONAUTICS

RESEARCH MEMORANDUM

PRESSURE DRAG OF BODIES AT MACH NUMBERS UP TO 2.0

By Robert L. Nelson and William E. Stoney, Jr.

The drag of bodies has now assumed greater importance because, as shown in references 1 and 2, the transonic drag rise of an airplane can be the same as its equivalent body. Obviously, the airplane designer would like his airplane to have a low-drag equivalent body. This paper shows some of the factors which minimize the drag of bodies at transonic and supersonic speeds and shows some of the penalties caused by deviating from low-drag body shapes.

Drag reductions can be obtained in two ways, first, through increasing the body fineness ratio, and second, through better shaping of the body profile at a given fineness ratio. The effects of fineness ratio are discussed first and then, more completely, detail-shape effects.

Largest reductions in body drag result from increases in body fineness ratio as is shown in figure 1. In figure 1 the variation of airplane drag with equivalent-body fineness ratio at $M = 1.05$ is plotted. In order to do this the pressure drag of an airplane is assumed to be the same as that of its equivalent body and C_D is based on wing area in order to get the results in more familiar terms. For the calculations, airplane volume and wing area are assumed to be constant. The values used are representative of a bomber-type airplane. The data points are from free-flight model tests of parabolic bodies having different maximum-diameter positions and base sizes (refs. 3 and 4). The curve simply connects the lower drag points. The difference between the total-drag curve and the friction-drag curve represents the minimum pressure drag for a given volume and fineness ratio for these body shapes. The minimum total-drag curve shows the large reduction in airplane drag obtained with an increase in equivalent-body fineness ratio. Largest reductions in drag occur at fineness ratios below 12 and the minimum drag occurs at about a fineness ratio of 24. This value will change somewhat for other Mach numbers and Reynolds numbers. Careful attention must be given to the nose and afterbody components which make up the body as indicated by the spread of test points at a given fineness ratio. Although not shown in figure 1, two wing-body configurations from reference 5 had approximately the same ratio of volume to wing area as that for the configurations represented in this plot. One configuration, of fineness ratio 6.5, had a C_D of 0.036 while the other, having an equivalent-body fineness ratio of 9 and a better shape, had a

C_D of 0.022. This effect of fineness ratio and the level of drag therefore is verified by the actual wing-body tests. The prime importance of fineness ratio on drag has been shown and the problem is now analyzed in more detail.

In figure 2 is shown the breakdown of a typical curve of drag coefficient plotted against Mach number for a body neglecting base drag. For bodies with bases, the base drag can be calculated by using the results of Love, Chapman, Cortright and Schroeder (refs. 6 to 8), and others. The friction drag can be calculated by the usual methods. The supersonic pressure drag for good bodies can be calculated at Mach numbers above that for shock attachment M_S by the second-order theory of Van Dyke (ref. 9). This paper considers mainly the range of Mach number below M_S , where the problem is difficult to analyze theoretically. This range is defined by the Mach number for peak drag M_P and the drag-rise Mach number M_{DR} .

Figure 3 shows correlations of drag-rise and peak-drag Mach numbers for a number of parabolic bodies (refs. 3 and 4). For the upper series of test points the Mach number for peak drag is plotted against nose fineness ratio. The curve shown is the Mach number for shock attachment to parabolic noses. The curve and the test points show the same general trend and indicate the dependence of the Mach number for peak drag on the Mach number for shock attachment.

For the lower series of test points, the drag-rise Mach number is plotted against the nose or afterbody fineness ratio, whichever is the least. The nose and afterbody test points fall within the same band and indicate that the drag-rise Mach number may be determined by either the nose or afterbody and is dependent mainly on fineness ratio.

Before discussing the peak drag of bodies, an examination is made of some of the effects of nose shape on drag at various Mach numbers. Figure 4 shows the drags of a number of fineness-ratio-3 noses. Although drags at this fineness ratio are relatively high, this fineness ratio was chosen so that the drag increments between the different shapes were more easily measurable. The results are presented in bar-graph form at $M = 1.05$, 1.24 , and 2.0 . The nose shapes include the cone, the parabolic nose having its vertex at maximum diameter, the L-V Haack nose (designed for minimum drag for a given volume and length), the hypersonic optimum or $x^{3/4}$ nose, the Von Kármán nose (designed for minimum drag for a given length and diameter), and the $x^{1/2}$ nose (which is a parabolic nose having its vertex at the tip). At $M = 1.05$, the results are from free-flight model tests from the Langley helium gun (at the testing station at Wallops Island, Va.); at $M = 1.24$ and 2.0 , the results are from the Ames 1- by 3-foot supersonic tunnel (ref. 10) except for the parabolic nose. For the parabolic nose, the results are from second-order theory.

At $M = 1.05$, the $x^{1/2}$ nose, which has a relatively blunt tip, has the least drag and is followed by the Von Kármán nose. At $M = 1.24$, the same result holds true. At $M = 2$, the hypersonic optimum nose has the least drag. This result also holds true at Mach numbers greater than 2. The $x^{1/2}$ nose at $M = 2$ has higher drag as a result of its blunt tip.

Although the Von Kármán nose has good drag characteristics over the Mach number range tested, it must be remembered that this nose was derived for vanishing thickness. For finite thickness, this slender-body-theory result does not apply. Recent work at the Langley Laboratory has solved the minimum-drag problem for finite thickness by using linearized theory. The resulting nose shapes have finite slopes at their maximum diameters.

Another indication that noses with finite slope at maximum diameter can have lower drag than noses with zero slope at maximum diameter is shown by some results for a family of noses generated by parabolic arcs. In figure 5 the nose pressure-drag coefficient is plotted against the shape parameter K which is related to the slope of the nose at maximum diameter. For $K = 1$, the parabolic nose has zero slope at maximum diameter. Reducing K gives slope at maximum diameter and for $K = 0$, the result is a cone. Both helium-gun tests at $M = 1.2$ and second-order theory at $M = 1.4$ show the same trend; therefore, minimum drag in the vicinity of $K = 0.7$ is indicated. This result indicates that, for parabolic noses, removing the restriction of zero slope at maximum diameter has resulted in a reduction in nose drag. For complete bodies, the reduction of nose drag by the use of such shapes may be offset by a greater interference drag of the nose on the afterbody.

In order to obtain an explanation of this drag reduction, the geometrical changes in the noses with a change in the shape parameter K have been examined. Examination of the nose profile shapes and the nose area distributions yielded no significant clues. However, the slopes of the nose-area-distribution curves give an important result as is shown in figure 6.

The nondimensional slope of the nose area distribution is plotted against nose station x/l for a number of values of K . Note that in going from $K = 1.0$ to 0.75 , the peak slope of the area distribution curve is reduced, whereas a further decrease of K to 0.5 and to 0 causes an increase in the peak slope; therefore, the lowest drag nose has the lowest peak slope. In figure 5 is also shown the drag value at $M = 1.2$ for the $x^{1/2}$ nose, which had the lowest drag at low supersonic speeds of all the noses presented earlier. The slope of the area-distribution curve for the $x^{1/2}$ nose is the lowest value possible and is constant as is shown in figure 6. Thus, from this experimental and theoretical study of the effect of nose shape on drag, the peak slope of the area-distribution curve is seen to be an important parameter which

influences the drag at low supersonic speeds. This parameter has less importance at higher Mach numbers since the $x^{3/4}$ nose with a relatively high peak slope had the least drag at $M = 2$.

A correlation of the peak drag of bodies using as part of the correlation parameter a function which is proportional to the slope of total body-area-distribution curve has been made.

Figure 7 shows 39 body shapes included in the drag correlation for smooth bodies. The bodies have different fineness ratios, maximum-diameter locations, base sizes, and profile shapes. In figure 8 the peak pressure-drag coefficient is plotted against a shape parameter which includes the function f which is related to the slope of the body-area-distribution curve, the base-diameter ratio, and an effective-body fineness ratio, which neglects any parallel portion of the body. The neglect of this cylindrical section presupposes small interference effects between the nose and afterbody. The drags of all the bodies are from free-flight model tests at high Reynolds numbers so that the flow is turbulent at both subsonic and supersonic speeds. The peak pressure drag was obtained by taking the difference between the peak total drag and the subsonic drag. For bodies having base areas greater than 20 percent of the maximum area, the drags were corrected for base pressure. Fin drag was subtracted for all models. The peak pressure drag correlates well by using this correlation parameter; this correlation indicates that for these body shapes the interference drag is small. The one body for which the correlation is poor has a low-fineness-ratio, highly convergent afterbody. This correlation is similar to a transonic drag correlation made by the Fort Worth Division of Convair in that the slopes of the area distributions are weighted in the same manner.

Since the correlation appears good, one would obviously seek low drag, for a given fineness ratio, by minimizing the quantity $f - 2 \left(1 - \frac{d_b}{d_{max}} \right)$. However, this minimization cannot be done directly since base drag must be included and the proper combination of base size and afterbody length must be found for low drag.

Figure 9 shows the results of some tests (ref. 4) in which the afterbody drag included both afterbody pressure drag and base drag. The tests were made with free-flight models flown from the helium gun. The noses on all the models were of high fineness ratio to minimize the interference of the nose on the afterbody. The stabilizing fins were thin and swept back to reduce the interference drag between the fins and the afterbody and to minimize the effect of the fins on the base pressure. At $M = 1.05$, the test Reynolds numbers for all models were over 8×10^6 ; at these Reynolds numbers and with the presence of the fins, the flow at the base is turbulent and thus the results are representative of full-scale values.

Twelve bodies had parabolic afterbodies of three fineness ratios and four base sizes, whereas four additional models had conical afterbodies. In the left-hand plot of figure 9 at $M = 1.05$, the pressure plus base drag coefficient of the afterbody is plotted against the base radius ratio r_b/r_{max} for the three afterbody fineness ratios. The plot shows that, as the afterbody fineness ratio increases, the base size for minimum drag approaches zero. The right-hand plot shows the base size for low drag against afterbody fineness ratio. It can be seen that the three points fall on a straight line through $r_b/r_{max} = 1$ at $l/d = 0$, which corresponds to a conical boattail angle which is constant and equals 4.5° . This angle of 4.5° corresponds with previous ballistic experience. Since the afterbodies have bases at fineness ratios below 6, any jet flow through the base must not cause higher base drag.

By using this plot of base size for low drag against afterbody l/d in conjunction with the peak-drag correlation parameter, a series of bodies have been designed which should have low drag based on body frontal area at $M = 1.05$. The bodies had profiles of the $x^{1/2}$ shape with maximum diameters located so as to minimize the correlation factor f for a given base size.

However, drags of these supposedly reduced-drag bodies were no lower than those of the lowest drag parabolic bodies presented in figure 1. The drag reduction indicated by the correlation parameter therefore was not realized. A comparison of the peak pressure drags of two of these bodies with the drags predicted by the correlation is presented in figure 10. As indicated by the vertical distance between the mean line from the correlation and the data points, the predicted drags are 40 to 60 percent below the actual values. This difference is due to interference between the nose and afterbody components. The 39 bodies for which the data correlated well had either zero slope of the nose at maximum diameter or had finite slope followed by a long parallel portion; as a result, the interference drag was small. However, for these two models, the nose with finite slope at maximum diameter was followed by the afterbody which also had finite slope at maximum diameter. Also shown in figure 10 is the peak-pressure drag for a body having the same nose and afterbody components as the fineness-ratio-8.91 body, but with a fineness-ratio-3.59 parallel portion. The drag of this body falls on the correlation curve and indicates that the interference drag has been greatly reduced. As a result the correlation should be used with caution in designing low-drag bodies for body shapes for which the interference drag can be high. A qualitative estimate of the interference drag between the nose and afterbody is given in a recent paper by Fraenkel (ref. 11).

Up to this point only smooth bodies have been discussed. Designing an airplane to a good area distribution, however, is difficult and bumps may occur in the area-distribution curve. Figure 11 shows the area distributions of twelve bumpy bodies which were equivalent bodies of airplane

configurations. In order to get a rough indication of the effects of the bumps on the drag, a comparison of the drag for each model with that for a parabolic body having the same length, maximum diameter, maximum-diameter location, and base size was made. Figure 12 shows a plot of the measured peak pressure drags of the twelve bumpy bodies against the peak pressure drags of the corresponding parabolic bodies, calculated by using the correlation shown earlier. The vertical distance from the dashed line to the data point represents the drag increment due to the bump. Except for one case, the drags of the bumpy bodies are from about 20 to 60 percent greater than for the parabolic bodies. The one case for which the drag of the bumpy body appears lower probably results from the fact that the drag of the bumpy body is low as a result of separation of flow over the afterbody, and, of course, the calculation of the parabolic-body drag does not account for this effect.

Since the effects of the bumps can be large, it is of interest to see whether the peak-drag correlation for smooth bodies will hold for bumpy bodies.

Figure 13 shows the peak-drag correlation for the twelve bumpy bodies. The peak pressure drag was obtained in the same manner as for the smooth bodies except that an additional correction was made for bodies with forward-facing steps in the area-distribution curves. It was assumed that the pressure over the step area corresponded to the pressure rise through an oblique shock ahead of a two-dimensional forward-facing step as given in a recent paper by Love (ref. 6). The peak drags for the bumpy bodies show the same trends as for smooth bodies; however, the scatter about the mean curve is much greater. Again, two bodies with highly convergent low-fineness-ratio afterbodies do not agree with the correlation.

The drag-rise Mach numbers for these twelve bodies followed the same trend as for the parabolic bodies shown earlier. The Mach numbers for peak drag were more complex, being more a function of detail nose geometry, than for the smooth bodies.

In conclusion, first, largest reductions in drag are possible through increases in both total-body fineness ratio and the fineness ratio of the component parts. Second, the drag-rise Mach number is dependent mainly on the fineness ratio of the shortest body component, whereas the Mach number for peak drag is a function of nose fineness ratio and shape.

Third, the peak drags of smooth bodies and bumpy bodies can be correlated by using a simple parameter which depends only on body shape if the interference drag is small.

Langley Aeronautical Laboratory,
National Advisory Committee for Aeronautics,
Langley Field, Va., September 11, 1953.

REFERENCES

1. Whitcomb, Richard T.: Recent Results Pertaining to the Application of the "Area Rule." NACA RM L53I15a, 1953.
2. Jones, Robert T.: Theory of Wing-Body Drag at Supersonic Speeds. NACA RM A53H18a, 1953.
3. Hart, Roger G., and Katz, Ellis R.: Flight Investigations at High-Subsonic, Transonic, and Supersonic Speeds To Determine Zero-Lift Drag of Fin-Stabilized Bodies of Revolution Having Fineness Ratios of 12.5, 8.91, and 6.04 and Varying Positions of Maximum Diameter. NACA RM L9I30, 1949.
4. Stoney, William E., Jr.: Some Experimental Effects of Afterbody Shape on the Zero-Lift Drag of Bodies for Mach Numbers Between 0.8 and 1.3. NACA RM L53I01, 1953.
5. Smith, Norman F., Bielat, Ralph P., and Guy, Lawrence D.: Drag of External Stores and Nacelles at Transonic and Supersonic Speeds. NACA RM L53I23b, 1953.
6. Love, Eugene S.: The Base Pressure at Supersonic Speeds on Two-Dimensional Airfoils and Bodies of Revolution (With and Without Fins) Having Turbulent Boundary Layers. NACA RM L53C02, 1953.
7. Chapman, Dean R.: An Analysis of Base Pressure at Supersonic Velocities and Comparison With Experiment. NACA Rep. 1051, 1951. (Supersedes NACA TN 2137.)
8. Cortright, Edgar M., Jr., and Schroeder, Albert H.: Investigation at Mach Number 1.91 of Side and Base Pressure Distributions Over Conical Boattails Without and With Jet Flow Issuing From Base. NACA RM E51F26, 1951.
9. Van Dyke, Milton Denaan: Practical Calculation of Second-Order Supersonic Flow Past Nonlifting Bodies of Revolution. NACA TN 2744, 1952.
10. Perkins, Edward W., and Jorgensen, Leland H.: Investigation of the Drag of Various Axially Symmetric Nose Shapes of Fineness Ratio 3 for Mach Numbers From 1.24 to 3.67. NACA RM A52H28, 1952.
11. Fraenkel, L. E.: The Theoretical Wave Drag of Some Bodies of Revolution. Rep. No. Aero. 2420, British R.A.E., May 1951.

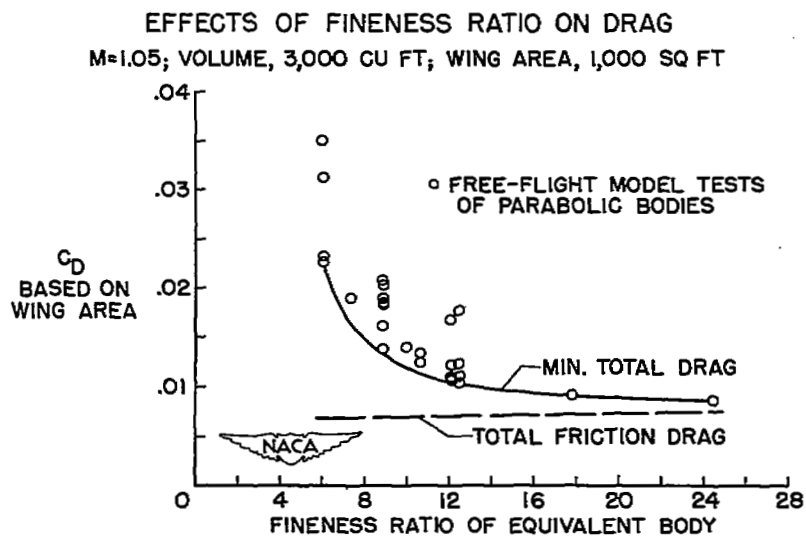


Figure 1

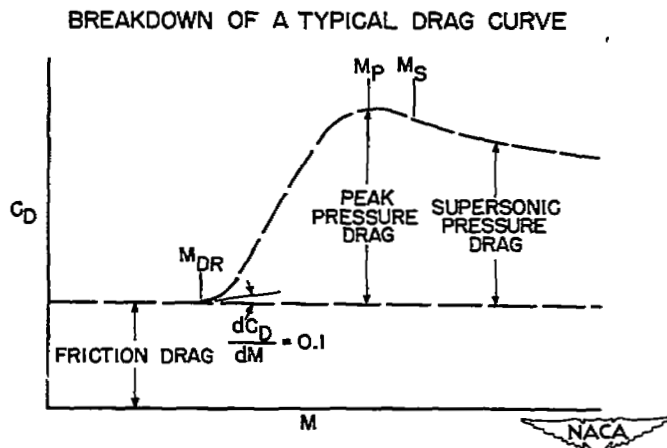


Figure 2

DRAG RISE AND PEAK DRAG MACH NUMBERS
PARABOLIC BODIES

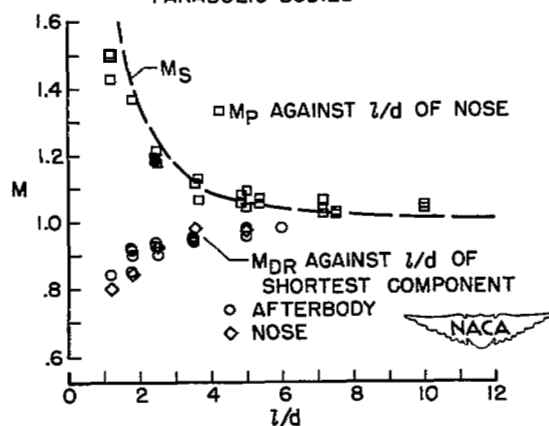


Figure 3

EFFECT OF NOSE SHAPE ON DRAG
 $l/d = 3$

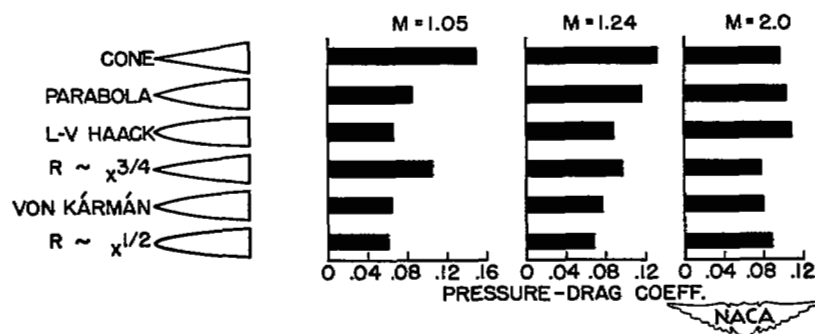


Figure 4

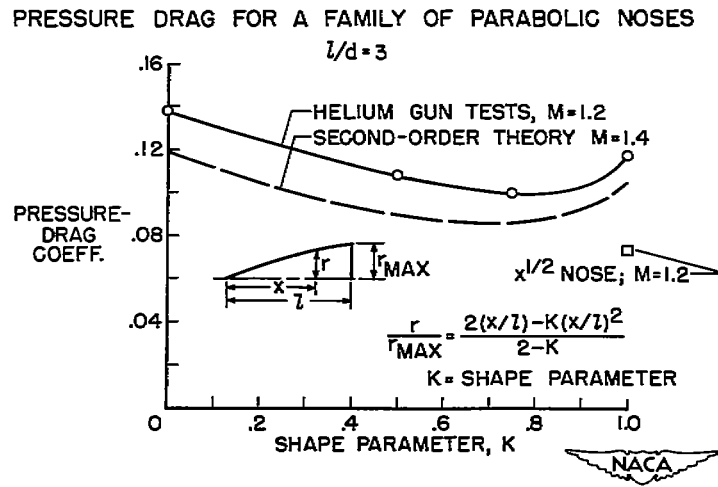


Figure 5

SLOPE OF AREA-DISTRIBUTION CURVE

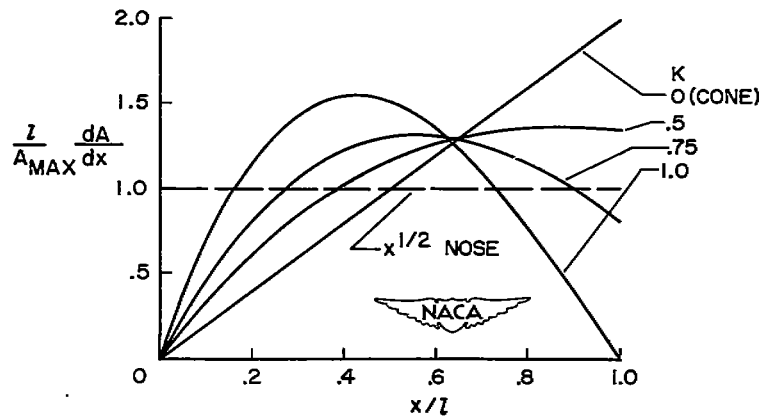


Figure 6

SMOOTH BODIES IN PEAK-PRESSURE-DRAG CORRELATION

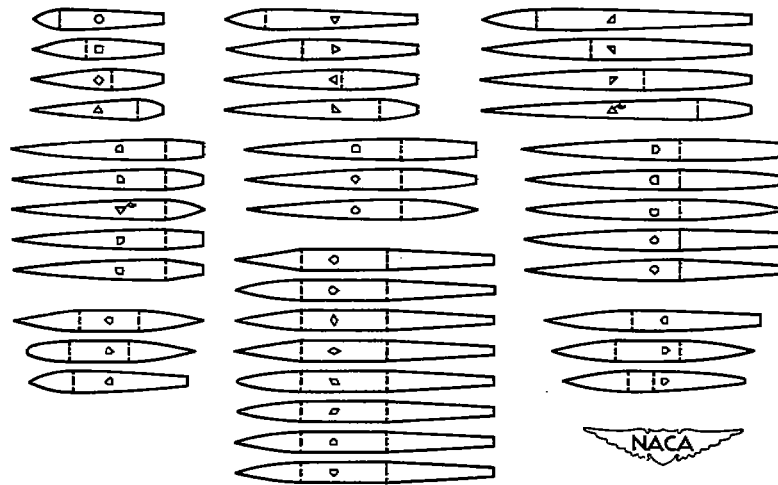


Figure 7

PEAK PRESSURE DRAG FOR SMOOTH BODIES

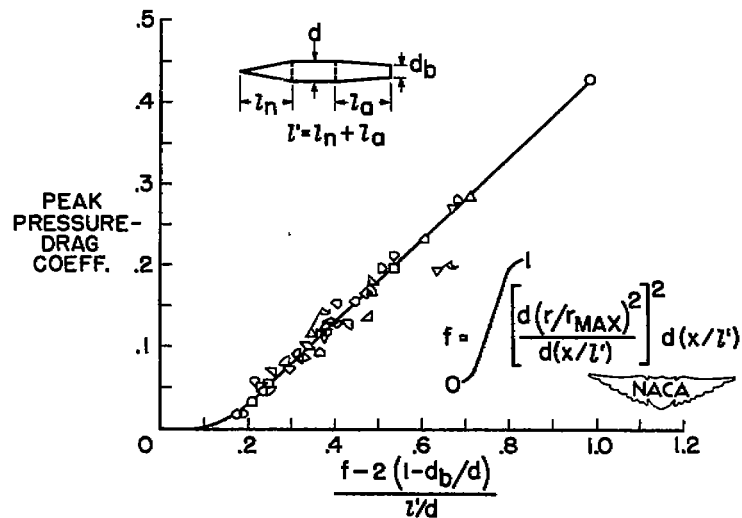


Figure 8

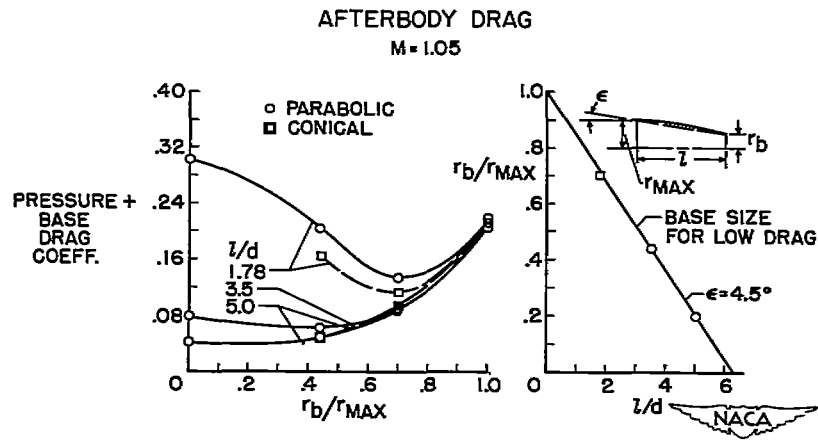


Figure 9

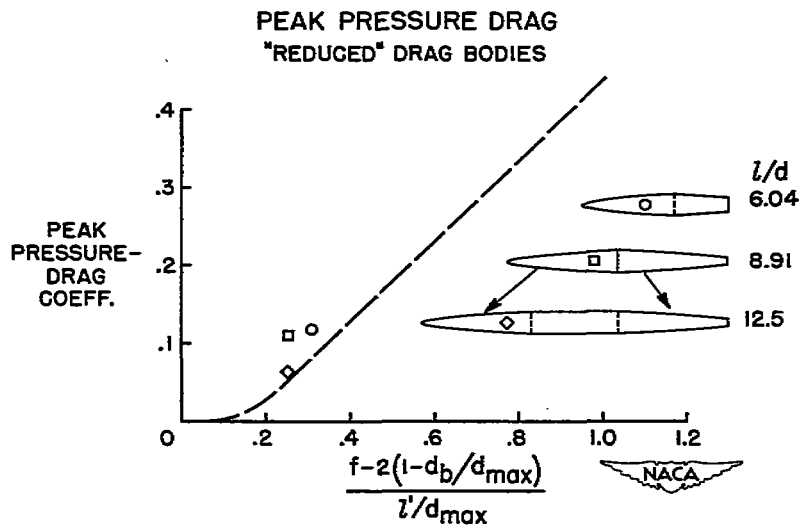


Figure 10

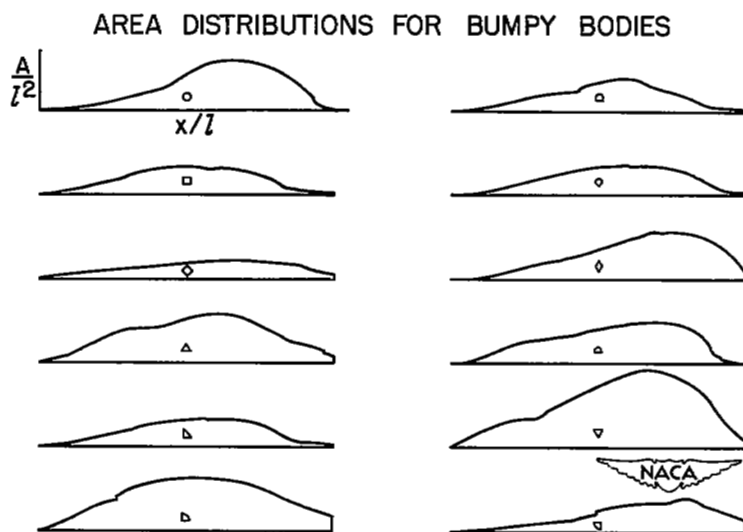


Figure 11

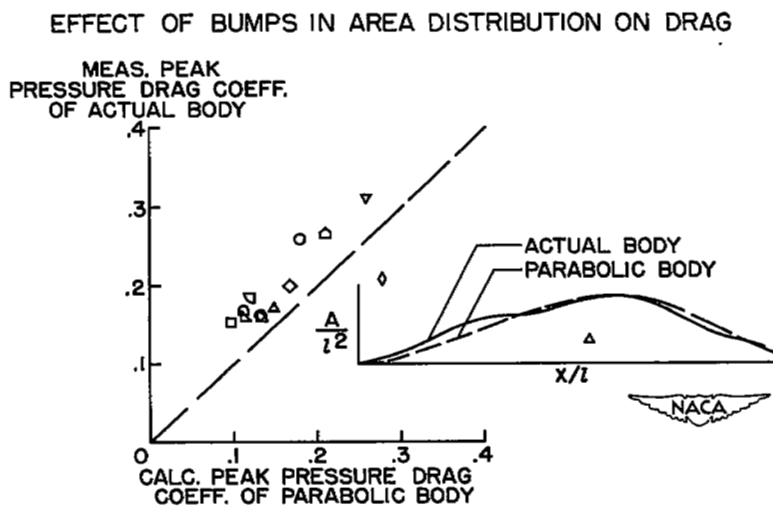


Figure 12

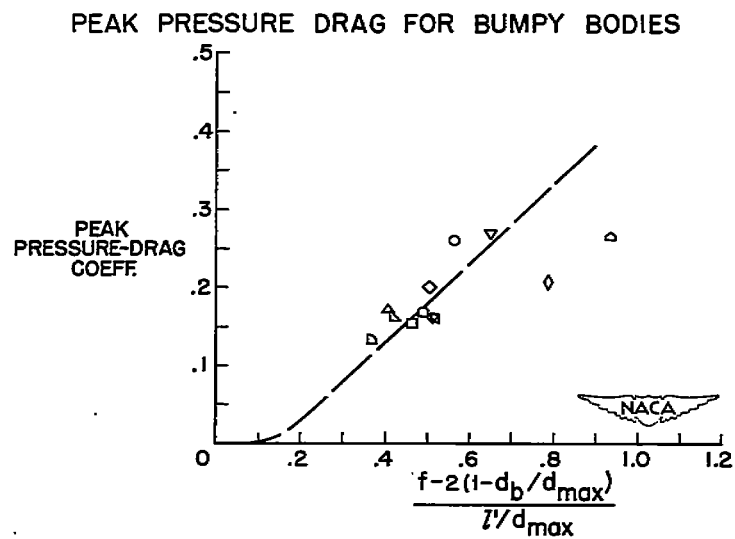
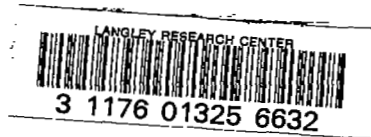


Figure 13

SECURITY INFORMATION



DO NOT REMOVE SLIP FROM MATERIAL

Delete your name from this slip when returning material to the library.

NAME	MS
<i>Tracy J.</i>	
<i>Retiree</i>	

NASA Langley (Rev. May 1988)

RIAD N-75